Editorial | Uncover This Tech Term

eISSN 2005-8330
https://doi.org/10.3348/kjr.2023.0743
Korean J Radiol 2023;24(12):1293-1297

Korean Journal of Radiology
KJR

Uncover This Tech Term: Compressed Sensing Magnetic Resonance Imaging

Sungjin Yoon[1], So Hyun Park[1], Dongyeob Han[2]

[1]Department of Radiology, Gil Medical Center, Gachon University College of Medicine, Incheon, Republic of Korea
[2]Siemens Healthineers Ltd., Seoul, Republic of Korea

Keywords: Magnetic resonance imaging; Compressed sensing; Undersampling; Reconstruction

Compressed sensing (CS) is a signal processing method that is utilized to reconstruct a signal from a small number of measurements [1]. CS has been employed to accelerate magnetic resonance imaging (MRI) acquisition [2]. Sparsity, pseudo-random undersampling, and non-linear iterative reconstruction are three essential components in CS.

Sparsity refers to the property in which only a minor portion of data hold information. For instance, most pixels in magnetic resonance cholangiopancreatography (MRCP) have dark signals, and only a few pixels represent the signal of the pancreaticobiliary duct. Therefore, MRCP is inherently sparse in the image domain. Most MRI images may appear complex in the image domain but can exhibit sparsity when transformed into an alternative domain [1,3]. Sparsity transforms like the wavelet transform identify relatively sparse components within images, which can be compressed with minimal information loss. This concept of sparsity transformation is a fundamental aspect of compressed sensing reconstruction.

Pseudo-random sampling is used in CS by increasing the sampling in the center of k-space [3]. In fact, pure random sampling is infeasible due to technical issues and a low signal-to-noise ratio (SNR) in CS. The pseudo-random sampling of k-space gives incoherency. Incoherent undersampling is employed in CS, leading to the generation of noise-like artifacts that become sparse in the wavelet domain. This is the main difference from parallel imaging, which exhibits a coherent (linear) k-space undersampling associated with aliasing artifacts.

Received: August 9, 2023 **Revised:** September 9, 2023
Accepted: September 10, 2023
Corresponding author: So Hyun Park, MD, PhD, Department of Radiology, Gil Medical Center, Gachon University College of Medicine, 21 Namdong-daero 774beon-gil, Namdong-gu, Incheon 21565, Republic of Korea
• E-mail: nnoleeter@gilhospital.com

Image Reconstruction with CS

Figure 1 illustrates the concepts and sequences of pseudo-random sampling, sparsity, and iterative reconstruction in CS.

1) Initially, k-space is measured with incoherent undersampling (y).

2) The measured k-space (y) is transformed into an image (x) using the Fourier transform. Image (x) has a noise-like aliasing artifact.

3) The image is transformed into a sparse domain. The image (x) exhibits sparse representation (Ψx) through the wavelet (using frequency splitting) transformation.

4) Inverse transformations are applied after thresholding the results in a denoised k-space. The regularization factor determines the noise threshold value in the sparse representation. Notably, thresholding in sparse representations reduces noise.

5) The denoised k-space after some processes is denoted as '(Ax)'. The data consistency can be verified by comparing (Ax) and the initially measured (y). Data consistency indicates how closely the denoised data match the initially measured data.

6) After checking data consistency, the Fourier transform is applied, and the denoised image from the current

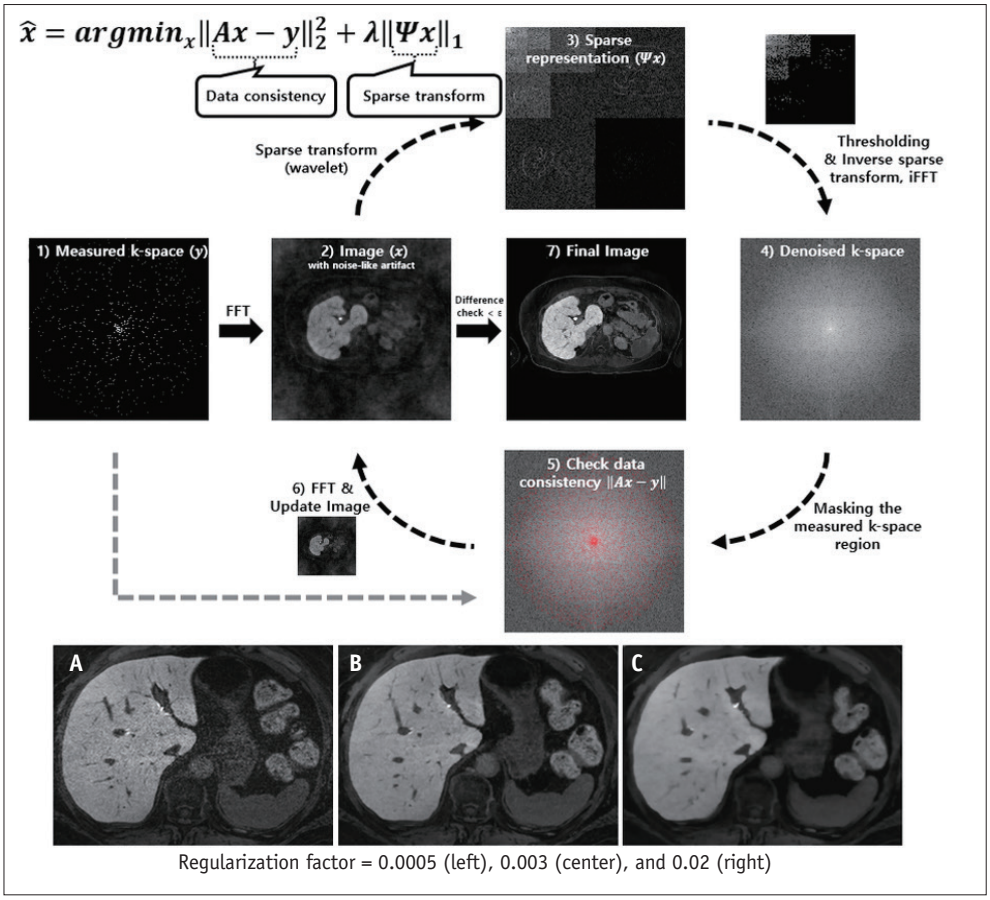

Fig. 1. Formula and graphical description of compressed sensing. **A-C:** Hepatobiliary phase magnetic resonance images of liver reconstructed by compressed sensing with different regularization factor (**A** = 0.0005, **B** = 0.003, **C** = 0.02). *argmin* = arguments of the minimum, y = measured k-space data, A = system function including fast Fourier transform (FFT) and coil sensitivity maps, x = target image to reconstruct, λ = regularization factor, Ψ = sparse transformation, iFFT = inverse FFT

iteration step is updated. The denoised image of the current iteration step is compared with that of the previous step.

7) If values of the differences from the images are smaller than the predefined threshold (ε), the updated image becomes the final image. Otherwise, iterative steps from 2) to 6) are repeated until the final image 7) is obtained.

Through an iterative reconstruction process, the reconstructed image $\hat{x}$ that satisfies the following equation is generated:

$$\hat{x} = argmin_x \|Ax\text{-}y\|_2^2 + \lambda \|\Psi x\|_1.$$

The $\|Ax\text{-}y\|_2^2$ represents data consistency and the $\|\Psi x\|_1$ represents sparsity. The regularization factor (λ) promoting sparsity in the transform domain ($\lambda \|\Psi x\|_1$) determines the weighting between data consistency and sparsity [4]. Increasing the regularization factor improves the perceived SNR of images (Fig. 1A, B), whereas images will be over-smoothed (Fig. 1C) and have an artificial appearance [4]. The identification of the optimal regularization factor is essential in CS.

Primary Advantage of CS

The CS technique allows for the use of a higher acceleration factor (AF) than conventional parallel imaging which typically uses an AF below 4, while maintaining image quality [5]. For example, using CS with 20 AF in MR acquisition will markedly reduce the scan time (1/20) compared to fully sampled images. Thus, the CS technique is utilized for rapid imaging while maintaining image quality or higher resolution without compromising the scan time [1,3,6].

https://doi.org/10.3348/kjr.2023.0743

Korean Journal of Radiology
KJR

Table 1. Clinical application of compressed sensing in the abdomen

	Respiratory mode	AF	Scan time, s	Conventional image*	Advantage	Disadvantage
MRCP	BH [7-12]	17–28[†]	13–20	x 17–27 faster	Higher visualization of the bile duct and pancreatic duct Better image sharpness owing to less motion-related imaging blurring	Lower background suppression Less accurate visualization of more delicate pancreatic duct structure Reduced image quality
	NT [7-10]	20–22[‡]	89–227	x 2–2.7 faster	Decreased motion-related artifacts owing to shorter acquisition time than conventional MRCP	Lower SNR
Liver dynamic image	BH [13,14]	4.76[§] [14], 7	18–19[‖], 16[‖]	NA	Higher acquisition rate of optimally timed late arterial phase without transient motion artifact	Noise-like incoherent artifacts Synthetic appearance
	FB [16,17]	6	11.6–11.8[¶]	NA	Allowing continuous data acquisition Applicable in patients with severe transient motion artifacts Reducing the burden of reexamination	Remnant respiratory motion artifacts
Static (HBP) image	BH [18-20]	4.5[§] [20], 8, 8.1	9–15	x 1.1–1.6 faster	Superior liver edge sharpness and focal lesion detectability with similar scan time Reduced scan time with comparable overall image quality and noninferior diagnostic performance	Nonrespiratory artifacts Subjective image noise
MRE, dynamic image	BH [15]	5[§]	11.5	x 1.5 faster	Higher sensitivity and accuracy for active inflammation of Crohn's disease Decreased motion and aliasing artifacts	Synthetic appearance Streak artifacts

*Scan speed compared to conventional imaging, [†]Acceleration factors in several studies include 17 (two studies), 20, 24 (two studies), and 28, and acquisition times were 13, 16 (two studies), 17 (two studies), and 20 s, [‡]Acceleration factors include 20 and 22 (three studies), and acquisition times are 134.1 ± 33.5 s (range: 89–204 s), 127.5 ± 36.9 s (range: 91–216 s), and 131.9 ± 33.6 s (range: 79–221 s), [§]Compressed sensing + parallel imaging, [‖]The scan time of three arterial phases is 18–19 s, and that of two arterial phases is 16 s, [¶]Temporal resolution is 11.6 and 11.8 s, respectively.
AF = acceleration factor, MRCP = magnetic resonance cholangiopancreatography, BH = breath-hold, NT = navigator-triggered, SNR = signal-to-noise ratio, FB = free breathing, NA = not available, HBP = hepatobiliary phase, MRE = magnetic resonance enterography

Clinical Applications of CS MRI: Abdominal Examples

MRCP

Applying the CS in MRCP enables a navigator-triggered (NT) or single breath-hold (BH) sequence to reduce the scan time in pancreatobiliary imaging (Table 1) [7-12]. In a few studies [7,10], BH-CS-MRCP demonstrated lower image quality, characterized by less accurate visualization of the delicate pancreatic duct, than NT-CS-MRCP or conventional NT-MRCP. However, recent studies have shown that CS-BH-MRCP exhibits comparable or better image quality than conventional NT-MRCP when using a 3T scanner or a smaller field of view [7,9-12].

Both BH- and NT-CS-MRCP have similar high AFs [7-12], whereas breath patterns and depth affect the longer scan time in NT-CS-MRCP (range, 89–227 s vs. 13–20 s). As BH-CS-MRCP reduces scan time and motion artifacts [9], it is currently widely used as an alternative or additional protocol to conventional NT-MRCP.

 https://doi.org/10.3348/kjr.2023.0743

Hepatic Imaging

Dynamic images obtained using the CS technique produce high-resolution BH [13-15] or free-breathing sequences (Table 1) [16,17]. Multiple arterial phase (AP) imaging using the CS technique within a single BH allows independent acquisition of k-space data at each AP. The BH-CS sequence resulted in a higher success rate for optimally timed late AP imaging than for single AP imaging [14]. Additionally, CS with multiple AP are more resistant to motion artifacts than single AP imaging or view-sharing techniques [13,14].

Dynamic T1-weighted images produce substantial motion artifacts in patients with limited BH capacity. Dynamic imaging using motion-state-resolved reconstruction (extra-dimensional volumetric interpolated breath-hold examination [XD-VIBE]) in a free-breathing manner allows continuous data acquisition and is useful for reducing the number of re-examinations [16,17]. XD-VIBE extends the CS concept by enforcing and exploiting sparsity along dynamic and respiration dimensions [16].

CS hepatobiliary phase (HBP) imaging exhibits improved resolution within a similar scan time [18,19] or comparable image quality with a reduced BH time [20] compared with conventional imaging (Table 1). A high AF (≥ 8) and optimized regularization factor enable a high spatial resolution of CS-HBP without increasing scan time, which demonstrates hyperintense liver parenchyma, superior liver edge sharpness, and superior focal lesion detectability [18,19]. However, a high AF may lead to remnant non-respiratory artifacts with image noise, even after iterations [18,19].

CONCLUSION

The application of CS techniques in clinical settings has improved the speed of abdominal imaging. By fine-tuning the acceleration and regularization factors using the CS technique, we can achieve enhanced image quality.

Conflicts of Interest

Dongyeob Han is an employee of Siemens Healthineers Ltd., however this do not affect to publish this manuscript. Other authors have no potential conflicts of interest to disclose.

Author Contributions

Conceptualization: So Hyun Park. Data curation: Sungjin Yoon, So Hyun Park. Investigation: Sungjin Yoon, So Hyun Park. Supervision: So Hyun Park. Validation: So Hyun Park, Dongyeob Han. Visualization: So Hyun Park, Dongyeob Han. Writing—original draft: Sungjin Yoon, So Hyun Park. Writing—review & editing: So Hyun Park, Dongyeob Han.

ORCID IDs

Sungjin Yoon
https://orcid.org/0000-0002-7030-841X
So Hyun Park
https://orcid.org/0000-0001-9935-2863
Dongyeob Han
https://orcid.org/0000-0002-1402-5036

Funding Statement

None

Acknowledgments

The authors would like to thank Munyoung Paek for technical support for MRI provided throughout this project.

REFERENCES

1. Donoho DL. Compressed sensing. *IEEE Transactions on Information Theory* 2006;52:1289-1306
2. Lustig M, Donoho D, Pauly JM. Sparse MRI: the application of compressed sensing for rapid MR imaging. *Magn Reson Med* 2007;58:1182-1195
3. Lustig M, Donoho DL, Santos JM, Pauly JM. Compressed sensing MRI. *IEEE Signal Processing Magazine* 2008;25:72-82
4. Sandino CM, Cheng JY, Chen F, Mardani M, Pauly JM, Vasanawala SS. Compressed sensing: from research to clinical practice with deep neural networks. *IEEE Signal Process Mag* 2020;37:117-127
5. Yoon JH, Nickel MD, Peeters JM, Lee JM. Rapid imaging: recent advances in abdominal MRI for reducing acquisition time and its clinical applications. *Korean J Radiol* 2019;20:1597-1615
6. Park CJ, Cha J, Ahn SS, Choi HS, Kim YD, Nam HS, et al. Contrast-enhanced high-resolution intracranial vessel wall MRI with compressed sensing: comparison with conventional T1 volumetric isotropic turbo spin echo acquisition sequence. *Korean J Radiol* 2020;21:1334-1344
7. Taron J, Weiss J, Notohamiprodjo M, Kuestner T, Bamberg F, Weiland E, et al. Acceleration of magnetic resonance cholangiopancreatography using compressed sensing at 1.5 and 3 T: a clinical feasibility study. *Invest Radiol* 2018;53:681-688
8. Zhu L, Wu X, Sun Z, Jin Z, Weiland E, Raithel E, et al. Compressed-sensing accelerated 3-dimensional magnetic resonance cholangiopancreatography: application in suspected pancreatic diseases. *Invest Radiol* 2018;53:150-157

https://doi.org/10.3348/kjr.2023.0743

9. Zhu L, Xue H, Sun Z, Qian T, Weiland E, Kuehn B, et al. Modified breath-hold compressed-sensing 3D MR cholangiopancreatography with a small field-of-view and high resolution acquisition: clinical feasibility in biliary and pancreatic disorders. *J Magn Reson Imaging* 2018;48:1389-1399
10. Yoon JH, Lee SM, Kang HJ, Weiland E, Raithel E, Son Y, et al. Clinical feasibility of 3-dimensional magnetic fesonance cholangiopancreatography using compressed sensing: comparison of image quality and diagnostic performance. *Invest Radiol* 2017;52:612-619
11. Chandarana H, Doshi AM, Shanbhogue A, Babb JS, Bruno MT, Zhao T, et al. Three-dimensional MR cholangiopancreatography in a breath hold with sparsity-based reconstruction of highly undersampled data. *Radiology* 2016;280:585-594
12. Song JS, Kim SH, Kuehn B, Paek MY. Optimized breath-hold compressed-sensing 3D MR cholangiopancreatography at 3T: image quality analysis and clinical feasibility assessment. *Diagnostics (Basel)* 2020;10:376
13. Kim JH, Yoon JH, Bae JS, Park S, Han S, Lee JM. Multiarterial phase acquisition in gadoxetic acid-enhanced liver MRI for the detection of hypervascular hepatocellular carcinoma in high-risk patients: comparison of compressed sensing versus view sharing techniques. *Invest Radiol* 2023;58:139-147
14. Yoon JK, Kim MJ, Lee S. Compressed sensing and parallel imaging for double hepatic arterial phase acquisition in gadoxetate-enhanced dynamic liver magnetic resonance imaging. *Invest Radiol* 2019;54:374-382
15. Kim J, Seo N, Bae H, Kang EA, Kim E, Chung YE, et al. Comparison of sensitivity encoding (SENSE) and compressed sensing-SENSE for contrast-enhanced T1-weighted imaging in patients with crohn disease undergoing MR enterography. *AJR Am J Roentgenol* 2022;218:678-686
16. Yoon JH, Yu MH, Chang W, Park JY, Nickel MD, Son Y, et al. Clinical feasibility of free-breathing dynamic T1-weighted imaging with gadoxetic acid-enhanced liver magnetic resonance imaging using a combination of variable density sampling and compressed sensing. *Invest Radiol* 2017;52:596-604
17. Park SH, Yoon JH, Park JY, Shim YS, Lee SM, Choi SJ, et al. Performance of free-breathing dynamic T1-weighted sequences in patients at risk of developing motion artifacts undergoing gadoxetic acid-enhanced liver MRI. *Eur Radiol* 2023;33:4378-4388
18. Yoon S, Shim YS, Park SH, Sung J, Nickel MD, Kim YJ, et al. Hepatobiliary phase imaging in cirrhotic patients using compressed sensing and controlled aliasing in parallel imaging results in higher acceleration. *Eur Radiol* 2023 Sep 21. [Epub]. https://doi.org/10.1007/s00330-023-10226-w
19. Choi MH, Kim B, Han D, Lee YJ. Compressed sensing for breath-hold high-resolution hepatobiliary phase imaging: image noise, artifact, biliary anatomy evaluation, and focal lesion detection in comparison with parallel imaging. *Abdom Radiol (NY)* 2022;47:133-142
20. Nam JG, Lee JM, Lee SM, Kang HJ, Lee ES, Hur BY, et al. High acceleration three-dimensional T1-weighted dual echo dixon hepatobiliary phase imaging using compressed sensing-sensitivity encoding: comparison of image quality and solid lesion detectability with the standard T1-weighted sequence. *Korean J Radiol* 2019;20:438-448